Saturated Behavior of the Gyrotron Backward-Wave Oscillator

S. H. Chen
National Center for High-Performance Computing, Hsinchu, Taiwan

K. R. Chu and T. H. Chang
Department of Physics, National Tsing Hua University, Hsinchu, Taiwan
(Received 20 January 2000)

Physical processes in the gyrotron backward-wave oscillator (gyro-BWO) are investigated theoretically. Results indicate highly current-sensitive field profiles and hence sharply contrasting linear and saturated behaviors. The linear field extends over the entire structure length, whereas the saturated profile depends strongly on the energetics in the internal feedback loop. It is shown that this distinctive feature substantially influences the basic properties of the gyro-BWO including the start-oscillation current, efficiency, power scaling, and stability of tuning.

PACS numbers: 84.40.Ik, 84.40.Fe

The gyrotron backward wave oscillator (gyro-BWO) is a promising source of coherent millimeter wave radiation based on the electron cyclotron maser instability on a backward waveguide mode (Fig. 1). The oscillation takes place as the forward moving electron beam and the backward wave form a feedback loop. This allows the gyro-BWO to employ a nonresonant structure; hence the frequency can be tuned over a wide band. Theoretical studies of the gyro-BWO first appeared in the mid-1960's in the Soviet literature, as has been reviewed in a recent paper [1]. Potential applications of a tunable millimeter-wave source include position selective heating of fusion plasmas, spectroscopy, materials processing, and drivers of ultrahigh power amplifiers. These prospects have motivated further theoretical [1–15] and experimental [16–24] investigations. Linear theory [4,6,13] forms the first theoretical basis by predicting the start-oscillation conditions. Orbit tracing techniques [1,8,9,14] and particle simulations [11,12,15] are then employed to investigate the nonlinear behavior. Uptapering the magnetic field [1,9,11,18,23] or downtapering the waveguide radius [23] has been shown to be effective means for efficiency enhancement. Megawatt output power levels have been achieved with high voltage and high current beams [19,22–24]. The injection locking technique has also been demonstrated for phase control and spectral purity [20].

Model, assumptions, and numerical method.—The current analysis addresses several issues concerning the linear and the nonlinear behavior of the gyro-BWO. We model the gyro-BWO by the configuration shown in Fig. 2(a). It consists of a uniform interaction section of length L connected at both ends, by a weak taper, to a short uniform section of slightly larger radius. The whole structure is immersed in a uniform magnetic field. All dimensions are fixed (at values shown in the figure) except for the uniform section length L which will be varied. The end tapers of Fig. 2(a) model the couplers of our earlier experiment [20] designed for broadband coupling. Although details of the end structure vary from device to device, the overall effect will be a small amount of wave reflection at the structure nonuniformity as well as some weak beam-wave interactions in the end structure itself, both being modeled here. Weaker beam-wave interaction in the upstream tapered region results in less abrupt initial electron bunching and hence higher efficiency as will be shown later.

In the standard treatment, self-oscillation of the backward wave is formulated as a condition of infinite gain. Hence, a zero-field point is imposed at the downstream end. This condition is convenient for implementation into linear theories and it is valid when the downstream field tapers down to small values. However, the zero-field condition precludes an outgoing or evanescent wave at the downstream end. Furthermore, in large signal operation there is no reason that the zero-field point should be at a fixed axial position, or even be present at all. Here we impose the more physical outgoing-wave boundary conditions [25]. Under such conditions, any solution that exists must then be one of self-oscillation. Since at no point is the field restricted to a fixed value, it is allowed to relax to a self-consistent profile at any beam current.

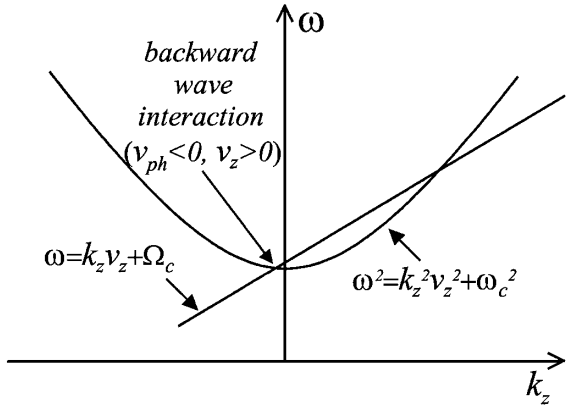

FIG. 1. ω-k_z diagram showing the operating point of the gyro-BWO. Ω_c, ω_c, and v_z are, respectively, the relativistic cyclotron frequency, cutoff frequency, and axial velocity of the electrons.

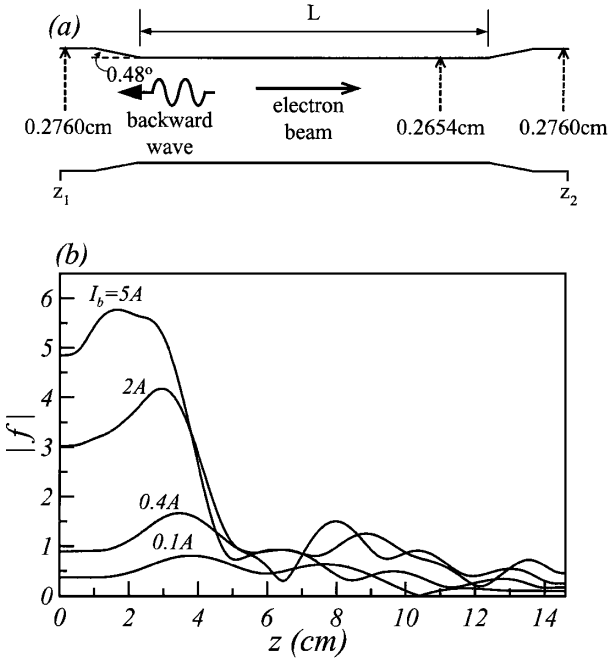

FIG. 2. (a) Configuration of the TE_{11} mode gyro-BWO under study. End structures are of fixed dimensions and the uniform section length L will be varied. (b) Evolution of the field profile (in relative scale) with increasing beam current I_b for $L = 10$ cm, $B_0 = 14.52$ kG, $V_b = 100$ kV, $\alpha = 1.0$, and $r_c = 0.09$ cm, where α is the electron pitch angle and r_c is its guiding center position. A cold beam is assumed. The oscillation frequency varies from 33.30 to 33.50 GHz as the current builds up from 0.1 to 5 A.

We assume the presence of a single (TE_{11}) mode. Let $f(z)$ be its complex field amplitude. On the left hand side ($z = z_1$), we specify

$$\frac{d}{dz} f(z_1) = -ik_z f(z_1), \tag{1}$$

where k_z is the local propagation constant and $\exp(-i\omega t)$ time dependence is assumed. The set of wave and electron dynamics equations [26] is then integrated axially from z_1 to z_2 by the orbit tracing technique. On the right hand side ($z = z_2$), we demand

$$\frac{d}{dz} f(z_2) = ik_z f(z_2). \tag{2}$$

Condition (2) is a complex equation to be solved by an iterative procedure for ω and $|f(z_1)|$, where ω gives the resonant frequency and $|f(z_1)|$ determines the output power. The absolute phase of $f(z_1)$ is of no consequence in the case of self-oscillations where only the relative phase matters. Condition (2) is equally valid for a cutoff end section, in which case k_z is purely imaginary corresponding to an evanescent wave.

Linear and saturated behavior.—Figure 2(b) shows the evolution of the field profile (for $L = 10$ cm) of the TE_{11} mode from the linear state ($I_b = 0.1$ A) to the saturated state ($I_b = 5$ A) as the beam current I_b increases. The profiles in various stages of nonlinearity are seen to exhibit very pronounced variations. Such variations result from the very nature of backward-wave interactions; namely, the upstream field derives its energy from the downstream interaction to form an internal feedback loop. As the field strength increases with the beam current, beam energy depletion due to an accelerated rate of extraction results in a contracted feedback loop, hence the concentration of the field near the beam entrance. This effect is important for the understanding and utilization of the properties of the gyro-BWO described below. It also marks a basic difference between the gyro-BWO and the gyromonotron. In the latter device, the reflective feedback loop extends end to end, in both the linear and nonlinear regimes.

For the fundamental axial mode, Fig. 3 displays the dependence of the saturated efficiency (maximized with respect to I_b) and the start-oscillation current I_{st} as functions of the length of the uniform section L (see Fig. 2). It shows a rapid drop of I_{st} with increased L, a property common to self-oscillating devices. However, in sharp contrast to such a linear property, the saturated efficiency (defined as the ratio of the backward output power to the beam power) depends very weakly on L. The oscillation frequency (shown later in Fig. 6) also remains nearly constant with respect to L. The constancy of the saturated efficiency and oscillation frequency can be understood in light of the saturated field profiles plotted in Fig. 4 for a fixed I_b and several values of L. It is seen that, regardless of the length L, the bulk of the field always concentrates toward the upstream end and assumes the same profile. Furthermore, as long as L exceeds a certain value (approximately half a guide wavelength for the fundamental axial mode), the bulk field always reaches the same amplitude [Figs. 4(b)–4(d)]. Any additional length beyond this value adds only a weak tail structure to the bulk field. We refer to the bulk width of the saturated field as the *relaxation length*. In saturated operations, the electron beam experiences a strong field immediately upon entering the interaction region. After traversing the bulk of the field, it becomes essentially a spent beam with large energy and velocity spreads. Hence, subsequent

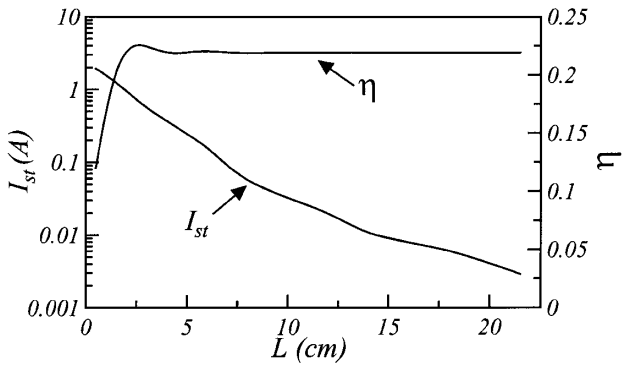

FIG. 3. Start-oscillation current (I_{st}) and saturated efficiency (η) versus the uniform section length L. Other parameters are the same as in Fig. 2.

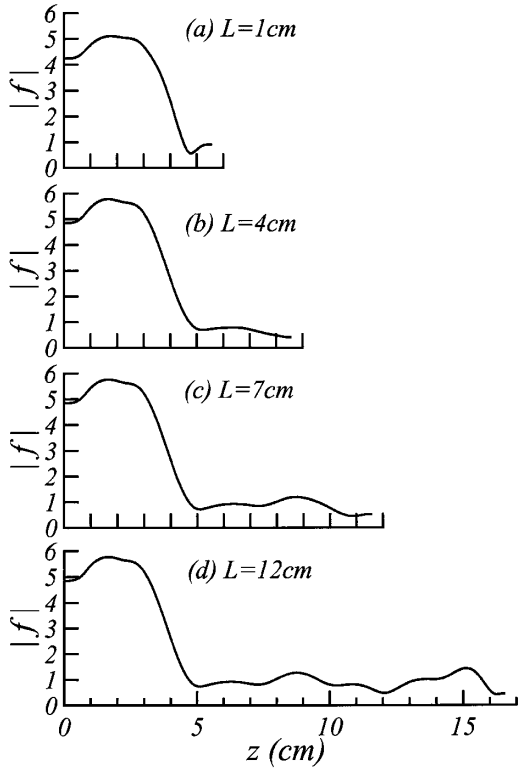

FIG. 4. Saturated field profile in relative scale plotted from z_1 to z_2 [see Fig. 2(a)] for (a) $L = 1$ cm, (b) $L = 4$ cm, (c) $L = 7$ cm, and (d) $L = 12$ cm. $I_b = 5$ A and other parameters are the same as in Fig. 2.

interaction with the tail portion of the field produces an insignificant effect to the saturated efficiency. The relaxation length is therefore the effective interaction length for saturated operations.

In the small signal regime, however, the wave field linearly modulates the electron energy (hence their cyclotron frequencies) which causes the beam to be increasingly bunched in the cyclotron phase space as it propagates down the tube. Hence, the downstream field interacts with a more tightly bunched beam. Because the downstream field now plays an effective role in the interaction processes, the longer the structure length, the more energy can be pumped into the field, resulting in a rapid drop of the start-oscillation current, as shown in Fig. 3.

Figure 5 plots the interaction efficiency versus I_b for different values of L. It shows, for each length L, the transition from the linear to the saturated state as I_b is raised. In Fig. 5, I_{st} is given by the point where the efficiency vanishes. It is interesting to note that from the lowest to the highest L value in Fig. 5, I_{st} varies by almost 2 orders of magnitude. Yet, despite the large variations of I_{st} with L, the efficiencies all reach the same peak value at approximately the same beam current as long as L exceeds the relaxation length (curves b, c, and d). This is a further indication that the structure length determines the linear behavior but an essentially constant relaxation length determines the saturated behavior.

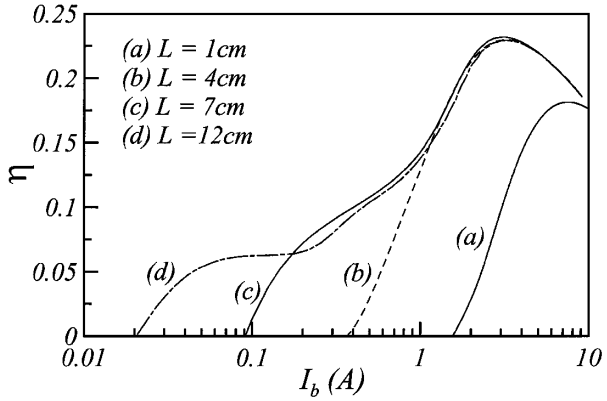

FIG. 5. Efficiency versus beam current for different values of L, showing sharply contrasting linear and saturated behaviors. Other parameters are the same as in Fig. 2.

Because the linear and nonlinear field profiles differ dramatically [Fig. 2(b)], the conventional relation between the saturation current (a nonlinear quantity) and the start-oscillation current (a linear quantity) becomes less and less meaningful as the structure length increases. This is a logical consequence of the effect of nonlinear field contraction. The fact that the saturation current can be significantly higher than the start-oscillation current therefore does not invalidate a steady-state solution as it does in the case of gyromonotron where the linear and nonlinear fields differ primarily in amplitude and assume essentially the same spatial profile. In fact, in one of our early gyro-BWO experiments [20], we employed a relatively long structure ($L = 17.5$ cm) for which the experimental operating current is about 500 times the theoretical start-oscillation current. The experimentally observed oscillation was sufficiently stable to allow phase locking with a drive power level of 27 dB below the saturated output [20].

Higher order axial modes.—We discussed here an implication of the results just presented. In most gyro-BWO experiments, ragged [18,20] or even discrete [21,24] power outputs were observed during the magnetic-field and voltage tuning of the frequency. Though not yet thoroughly investigated, interferences from the competing modes are thought to be a likely cause for such tuning curves.

Figure 6 shows the three lowest-order axial modes obtained for different uniform section lengths (L) and a fixed beam current of 5 A. The modes shown in Fig. 6 are the complete set of axial modes up to $L = 14$ cm. When $L > 14$ cm, there exist more higher order axial modes (HOMs) than shown in the figure. These additional HOMs become increasingly difficult to obtain numerically. It is seen in Fig. 6 that the number of HOMs increases with length L. As in the case of the fundamental mode and for the same reason, the saturated efficiency and the oscillation frequency for each HOM remain nearly constant as long as L exceeds a certain relaxation length.

The gyro-BWO experiments [15–23] reported so far employed a structure length ranging from 2 to 5 guide

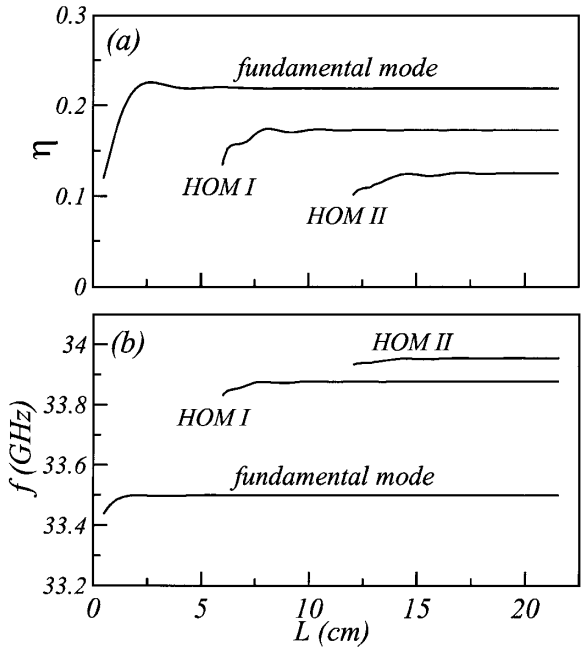

FIG. 6. Efficiency (a) and frequency (b) of axial modes versus the uniform section length L, showing an increasing number of axial modes as L increases. $I_b = 5$ A and other parameters are the same as in Fig. 2.

wavelengths, which corresponds to $L = 12$ to 30 cm in the scale of Fig. 6. Thus they all fell in the regime where a multiple of axial modes could be excited. Figure 2(b) suggests that these HOMs might be completely avoided at no expense to the interaction efficiency if one chooses an L value of approximately half a guide wavelength. We are currently conducting a gyro-BWO experiment with $L =$ 3 cm. Preliminary results have confirmed such predictions.

In summary, numerical modeling of the gyro-BWO with outgoing-wave boundary conditions has led to the physical insight of nonlinear contraction of the axial field profile, a property unique to the gyro-BWO and shown to be important for the realization of its optimum performance.

This work was supported by the National Science Council, Taiwan. The authors are grateful to Professor N. C. Luhmann, Jr. for his helpful comments.

[1] G. S. Nusinovich and O. Dumbrajs, IEEE Trans. Plasma Sci. **24**, 620 (1996).
[2] V. K. Yulpatov, Radiophys. Quantum Electron. **10**, 471 (1967).
[3] N. S. Ginzburg, I. G. Zarnitsyna, and G. S. Nusinovich, Radio Eng. Electron. Phys. (USSR) **24**, 113 (1979).
[4] J. M. Wachtel and E. J. Wachtel, Appl. Phys. Lett. **37**, 1059 (1980).
[5] V. L. Bratman, N. S. Ginzburg, G. S. Nusinovich, M. I. Petelin, and P. S. Strlkov, Int. J. Electron. **51**, 541 (1981).
[6] S. Y. Park, V. L. Granatstein, and R. K. Parker, Int. J. Electron. **57**, 1109 (1984).
[7] M. Caplan, in *Proceedings of the 12th International Conference on Infrared and Millimeter Waves* (SPIE–International Society for Optical Engineering, Bellingham, WA, 1987), p. 276.
[8] A. K. Ganguly and S. Ahn, Int. J. Electron. **67**, 261 (1989).
[9] A. K. Ganguly and S. Ahn, Appl. Phys. Lett. **54**, 514 (1989).
[10] G. Vasilakos, T. R. Stephenson, G. D. Ramlow, D. B. McDermott, N. C. Luhmann, Jr., and M. Caplan, in *Proceedings of the 16th International Conference on Infrared and Millimeter Waves* (SPIE–International Society for Optical Engineering, Bellingham, WA, 1991).
[11] A. T. Lin, Phys. Rev. A **46**, 4516 (1992).
[12] A. T. Lin and C. C. Lin, Phys. Fluids B **5**, 2314 (1993).
[13] C. S. Kou, Phys. Plasmas **1**, 3093 (1994).
[14] C. S. Kou, C. H. Chen, and T. J. Wu, Phys. Rev. E **57**, 7162 (1998).
[15] M. J. Arman, IEEE Trans. Plasma Sci. **26**, 693 (1998).
[16] S. Y. Park, R. H. Kyser, C. M. Armstrong, and R. K. Parker, in *Proceedings of the International Electron Device Meeting* (IEEE, New York, 1987), p. 933.
[17] W. C. Guss, K. E. Kreischer, R. J. Temkin, M. Caplan, and B. Kulke, in *Proceedings of the 14th International Conference on Infrared and Millimeter Waves* (SPIE–International Society for Optical Engineering, Bellingham, WA, 1989), p. 369.
[18] S. Y. Park, R. H. Kyser, C. M. Armstrong, R. K. Parker, and V. L. Granastein, IEEE Trans. Plasma Sci. **18**, 321 (1990).
[19] T. A. Spencer, R. M. Gilgenbach, and J. J. Choi, J. Appl. Phys. **72**, 1221 (1992).
[20] C. S. Kou, S. H. Chen, L. R. Barnett, H. Y. Chen, and K. R. Chu, Phys. Rev. Lett. **70**, 924 (1993).
[21] M. A. Basten, W. C. Guss, K. E. Kreischer, R. J. Temkin, and M. Caplan, Int. J. Infrared Millim. Waves **16**, 889 (1995).
[22] T. A. Spencer, C. E. Davis, K. J. Hendricks, F. J. Agee, and R. M. Gilgenbach, IEEE Trans. Plasma Sci. **24**, 630 (1996).
[23] M. T. Walter, R. M. Gilgenbach, J. W. Luginsland, J. M. Hochman, J. I. Rintamaki, R. L. Jaynes, Y. Y. Lau, and T. A. Spencer, IEEE Trans. Plasma Sci. **24**, 636 (1996).
[24] K. Kamada, K. Nawashiro, F. Tamagawa, H. Igarashi, S. Kizu, C. Y. Lee, S. Kawasaki, R. Ando, and M. Masuzaki, Int. J. Infrared Millim. Waves **19**, 1317 (1998).
[25] V. L. Bratman and M. A. Moiseev, Radiophys. Quantum Electron. **18**, 722 (1975).
[26] K. R. Chu, H. Y. Chen, C. L. Hung, T. H. Chang, L. R. Barnett, S. H. Chen, T. T. Yang, and D. Dialetis, IEEE Trans. Plasma Sci. **27**, 391 (1999).